DE GRUYTER OPEN

Substitutional effect of copper on the cation distribution in cobalt chromium ferrites and their structural and magnetic properties

TALAT ZEESHAN*, SAFIA ANJUM, HINA IQBAL, REHANA ZIA

Department of Physics, Lahore College for Women University, ail Road? Jubilee Town, Lahore, Punjab 54000, Pakistan

A series of copper substituted cobalt chromium ferrites, $Cu_xCo_{1-x}Cr_{0.5}Fe_{1.5}O_4$ (x = 0, 0.2, 0.4, 0.6, 0.8, 1.0) has been synthesized, by employing powder metallurgy method. Calcination of the samples has been carried out for 24 hours at 1100 °C. The resultant materials have been investigated by using a variety of techniques, including X-ray diffractometry (XRD), Fourier transform infrared spectroscopy (FT-IR), vibrating sample magnetometer (VSM)), scanning electron microscopy (SEM), and ultraviolet visible spectroscopy (UV-Vis). The XRD patterns confirmed that all compositions had a cubic spinel structure with a single phase and the lattice parameter was found to increase with increasing copper concentration. FT-IR spectroscopy has been used for studying the chemical bonds in the spinel ferrite. Shifting of the bands υ_1 and υ_2 has been observed. It has been revealed from VSM analysis that saturation magnetization and coercivity decrease with rising the Cu^{+2} doping. Magnetic properties have been explained on the basis of cation distribution. Scanning electron microscopy (SEM) has been used to study the surface morphology of prepared samples. UV-Vis analysis revealed the optical absorption of the samples. An increase in band gaps has been observed with increasing copper concentration in the sample.

Keywords: *crystal structure; ferromagnetic properties; optical band gap*

1. Introduction

Nowadays, cobalt ferrites are very famous hard magnetic material with relatively high saturation magnetization and coercivity, whereas nickel is a soft magnetic material with low values of these parameters. Most of these soft and hard magnetic properties make these materials useful for variety of applications in electronic devices and biotechnologies [1–4]. $CuFe_2O_4$ is a spinel ferrite which exhibits changing semi-conductive as well as switching properties [5]. Moreover, application-wise, magnetic behavior of nanoparticles depends upon their purity, size, shape and magnetic stability. The nanoparticles should be of single domains with suitable coercivity, moderate magnetization and pure phase values. That is why there is a requirement to tailor the magnetic properties of such type of materials. This is possible either by changing the particle size or by adjustment of hard and soft ferrite concentrations in these materials.

Though $CoFe_2O_4$ and $CuFe_2O_4$ has been a subject of numerous research papers, there are only few works about mixed Co–Cu ferrites. The synthesis of this mixed sample is mainly performed by sol-gel or co-precipitation method [6–9]. The electrical properties of cobalt ferrites change drastically with composition. Hence, they are frequently used to investigate the conduction mechanism in ferrites.

An effort has been made to investigate the structural, magnetic, morphological and optical properties of copper doped cobalt chromium mixed ferrites. Cobalt ferrite is used as an excellent core material for power transformers in electronic and telecommunication applications due to its high electric resistivity and good magnetic properties [10].

2. Experimental

The proposed $Cu_xCo_{1-x}Cr_{0.5}Fe_{1.5}O_4$ ferrites were prepared by powder metallurgy method. The samples were made by thoroughly mixing

---

*E-mail: talats@hotmail.com

a copper oxide, cobalt oxide, chromium oxide and iron oxide in the stoichiometric ratio and then grinded in a mortar with a pestle for few hours. The powder samples were calcined for 24 h at 1100 °C in a furnace and slowly cooled down to room temperature. The powders were then re-grinded to get fine powder and then pressed at a pressure of 400 MPa to prepare the green bodies. The pellets were finally sintered at 500 °C for 3 h to remove the organic binder.

3. Results and discussion

The prepared samples have been characterized by X-ray diffraction (XRD), Fourier transform infrared spectroscopy (FT-IR), vibrating sample magnetometer (VSM), scanning electron microscopy (SEM) and UV-Vis spectroscopy to study the structural, magnetic, surface morphology and optical properties.

3.1. X-ray diffraction analysis

XRD patterns of the sample $Cu_xCo_{1-x}Cr_{0.5}Fe_{1.5}O_4$ have been illustrated in Fig. 1. The crystal structure of calcined powder has been examined by an X-ray diffractometer with CuKα radiation.

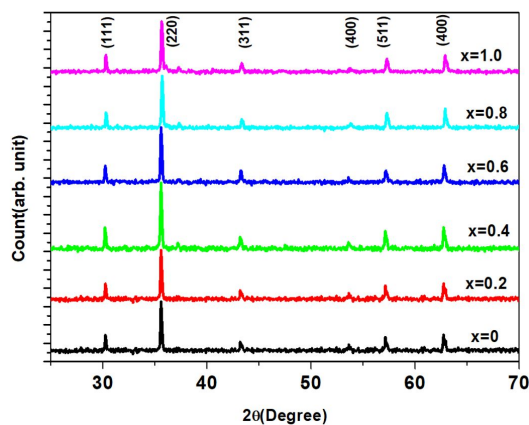Fig. 1. X-ray diffraction pattern of $Cu_xCo_{1-x}Cr_{0.5}Fe_{1.5}O_4$.

The X-ray powder diffraction patterns have been compared with JCPD data (CPDS Card No. 25-0283 and ICDD No. 79-1744b) for the phase assessment. The presence of (1 1 1), (2 2 0), (3 1 1), (4 0 0), (5 1 1) and (4 0 0) major planes confirms the formation of cubic spinel ferrites. The lattice parameter has been calculated by using the values of d spacing and respective (h k l) planes using the classical equation [11]:

$$a = \frac{\lambda \sqrt{(h^2 + k^2 + l^2)}}{4 \sin\theta} \qquad (1)$$

where 1.5406 Å is the wavelength of CuKα radiation and θ is the diffraction angle. The lattice constant decreases with increasing the Cu^{2+} concentration x which is listed in Table 1. The reason of this decreasing is the difference of ionic radii of Cu and Co, as the ionic radii of Co^{2+} (0.78 Å) are larger than that of Cu^{2+} (0.57 Å). This shows that Cu^{2+} ions have simply replaced the Co^{2+} ions in $Cu_xCo_{1-x}Cr_{0.5}Fe_{1.5}O_4$ samples. Thus, by the substitution of smaller Cu^{2+} ion with larger Co^{2+} ion causes the compression of unit cell.

The crystallite size has been calculated from line broadening of the most intense peak related to the (3 1 1) plane using Debye Scherrer formula [11]:

$$D_{hkl} = 0.9\lambda/\beta\cos\theta \qquad (2)$$

where D_{hkl} is crystallite size, λ is the wavelength of the radiation, β is full width at half maximum of corresponding peaks and θ is its angular position [12]. The crystallite size is found to decrease with increasing copper content. This may be due to the smaller ionic radius of Cu^{2+} than that of Co^{2+} ion. It is possible that the insertion of copper ion hinders the grain growth which causes the particle size reduction. On the other hand, by increasing the concentration of copper ions, the weak diffraction peak shows the presence of tetragonal structure of copper ferrites. These tetragonal distortions are caused by Jahn-Teller effect of Cu^{2+} ions situated in octahedral sites [13].

X-ray density of the sample has been calculated using the expression in equation 3:

$$D_x = 8M/Na^3 \qquad (3)$$

where M is the molecular weight of the sample, N (6.0225×10^{23}) is Avogadro number, 8 is

Table 1. Diffraction angle θ, full width at half maximum FWHM, d-spacing, lattice parameter a, crystallite size D and X-ray density of $Co_{1-x}Cu_xCr_{0.5}Fe_{1.5}O_4$.

Sample (x)	2θ [°]	FWHM [rad]	d-spacing [Å]	Lattice parameter [Å]	Crystallite size [nm]	Density [g/cm³]
0	35.55	0.68	2.52	8.36	12.62	5.27
0.2	35.61	0.18	2.52	8.35	47.11	5.33
0.4	35.65	0.17	2.52	8.35	59.72	5.37
0.6	35.62	0.18	2.52	8.35	47.11	5.37
0.8	35.81	0.18	2.50	8.30	48.71	5.49
1	35.62	0.83	2.52	8.35	10.50	5.43

the number of unit cells and a is the lattice constant. It can be observed from Table 1 that the value of X-ray density increases with increasing the Cu concentration. This may be due to the fact that copper has larger atomic weight (63.546 amu) than cobalt (58.933 amu) [14, 15]. Therefore, by replacing the copper with cobalt the volume is increasing which causes an increase in the X-ray density. The estimated cation distribution in prepared material and their preferent sites have been shown in Table 2.

It is clear from Table 2 that both Cu^{2+} and Co^{2+} ions prefer to occupy the octahedral sites, similarly, the Cr^{3+} ions also have strong preference to occupy the octahedral sites, whereas the Fe^{3+} ions are equally distributed among the tetrahedral and octahedral sites.

3.2. FT-IR analysis

The Fourier transform infrared spectroscopy gives information about local symmetry present in crystalline solids. According to Waldron [18], FT-IR spectra of the $Cu_xCo_{1-x}Cr_{0.5}Fe_{1.5}O_4$ (with x = 0, 0.2, 0.4, 0.6, 0.8, 1) in the range of 400 cm^{-1} to 1000 cm^{-1} have been shown in Fig. 2.

The FT-IR spectra show that the prepared ferrites consist of crystals permanently bound through covalent, ionic or van der Waals forces with the nearest neighbors.

FT-IR spectra of the ferrite samples reveal the presence of two main transmission bands in the range of 662 cm^{-1} to 657 cm^{-1} and 416 cm^{-1} to 414 cm^{-1} which are tabulated in Table 3.
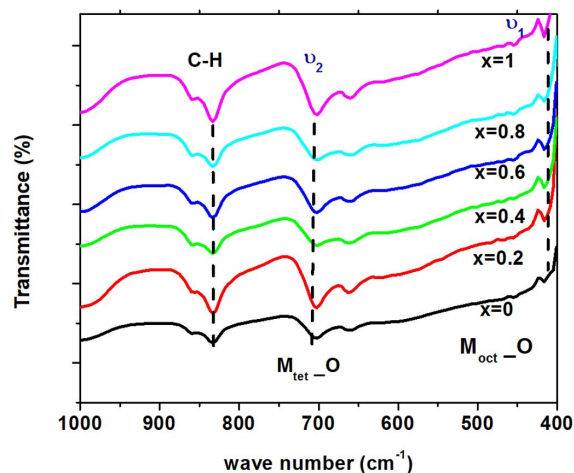

Fig. 2. FT-IR spectra of $Cu_xCo_{1-x}Cr_{0.5}Fe_{1.5}O_4$ compound with changing content of Cu.

It is known that Co^{2+} and Cr^{3+} ions preferentially occupy octahedral-site, while Fe^{3+} ions can occupy both octahedral and tetrahedral sites [17, 18]. It is to be noted from the spectra that both υ_1 and υ_2 slightly shift towards lower frequencies with increasing Cu^{2+} ions concentration

The substitution of Cu^{2+} ions (0.70 Å) in the system decreases the amount of Co^{2+} (0.78 Å) and increases the amount of Fe^{3+} (0.67 Å) ions in the octahedral B-sites. Thus, the replacement of cobalt ions with copper ions, which have small atomic mass and lesser ionic radius, at the octahedral sites B, is the main reason of the observed shift in the υ_2 band position. Similarly, Cu^{2+} ions sometimes occupy tetrahedral sites, which causes a change in υ_1 band position. The magnetic ion distance at A site

Table 2. Cationic distribution estimated for $Co_xCu_{1-x}Cr_{0.5}Fe_{1.5}O_4$ using XRD analysis.

Sample x	Tetrahedral site	Octahedral site
0.0	$Co_{0.3}Fe_{0.7}$	$Co_{0.7}Cr_{0.5}Fe_{0.8}$
0.2	$Co_{0.3}Cu_{0.1}Fe_{0.7}$	$Co_{0.5}Cu_{0.1}Cr_{0.5}Fe_{0.9}$
0.4	$Co_{0.3}Cu_{0.2}Fe_{0.6}$	$Co_{0.2}Cu_{0.3}Cr_{0.5}Fe_{0.9}$
0.6	$Co_{0.1}Cu_{0.2}Fe_{0.7}$	$Co_{0.3}Cu_{0.4}Cr_{0.5}Fe_{0.8}$
0.8	$Co_{0.2}Cu_{0.2}Fe_{0.6}$	$Co_{0.3}Cu_{0.3}Cr_{0.5}Fe_{0.9}$
1.0	$Cu_{0.1}Fe_{0.9}$	$Cu_{0.7}Cr_{0.5}Fe_{0.8}$

Table 3. IR bands, force constants and bond lengths for $Cu_xCo_{1-x}Cr_{0.5}Fe_{1.5}O_4$ sample.

Sample (x)	υ_2 [cm^{-1}]	υ_1 [cm^1]	K_1 [N/m]	K_2 [N/m]	L_A [Å]	L_B [Å]
0	415	658	187	101.8	3.625	2.955
0.2	414	660	188	102.3	3.624	2.949
0.4	414	662	188	102.4	3.618	2.947
0.6	416	661	193	109.9	3.616	2.947
0.8	415	657	192	103.7	3.616	2.944
1.0	415	660	192	103.7	3.613	2.884

and B sites can be calculated from $L_A = a(3)^{1/2}/4$ and $L_B = a(2)^{1/2}/4$, respectively. It has been clearly observed that both L_A and L_B depend upon the values of a and they decrease with increasing the copper content, which may possibly be due to unit cell enlargement arising from the replacement of smaller radius copper ion with larger radius cobalt ion. The force constants related to tetrahedral complexes and octahedral complexes can be calculated using the formula [19]:

$$K_1 = 7.62 \cdot M_1 \cdot \upsilon_1^2 \cdot 10^{-7} \text{N/m} \qquad (4)$$

$$K_2 = 10.62 \cdot M_2 \cdot \upsilon_2^2 \cdot 10^{-7} \text{N/m} \qquad (5)$$

where K_1 and K_2 are the force constants of tetrahedral and octahedral sites, M_1 and M_2 are the molecular weights of corresponding tetrahedral and octahedral sites which have been calculated from the estimated cation distribution. Similarly υ_1 and υ_2 are the center frequency of tetrahedral and octahedral sites. The values of force constants and bond lengths are given in Table 3. It is to be noticed that the values of force constants have increased and bond lengths decrease with increasing the copper concentration which is shown in Fig. 3. It is recognized that the bond lengths (L_A, L_B) are inversely

proportional to the force constant which suggests that with increasing the copper concentration the inter-atomic distance decreases [20].
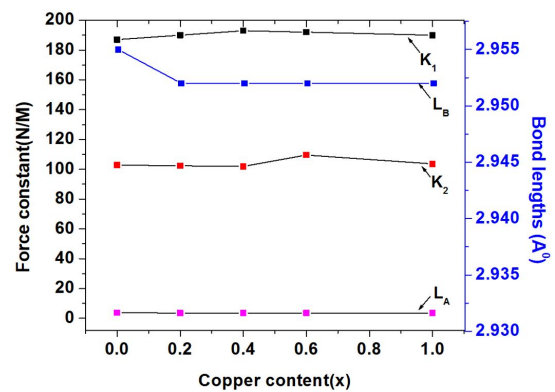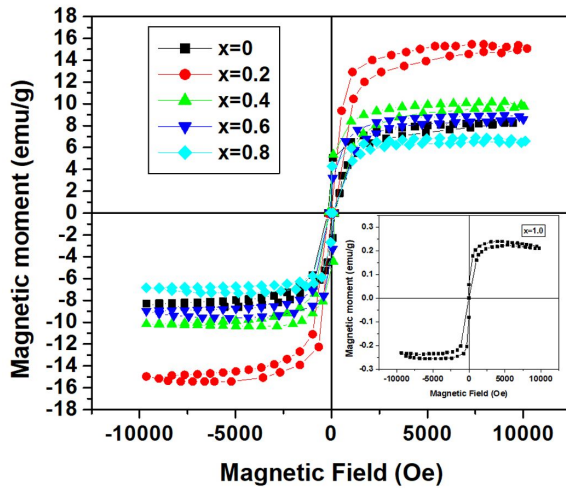

Fig. 3. Force constants and bond lengths versus copper content.

3.3. VSM analysis

Hysteresis loops of prepared $Cu_xCo_{1-x}Cr_{0.5}Fe_{1.5}O_4$ samples of all the compositions are shown in Fig. 4. The parameters, such as coercivity, saturation magnetization, retentivity and anisotropic constant calculated from the hysteresis loop, are listed in Table 4.

Table 4. Parameters extracted from VSM analysis.

Sample (x)	Saturation magnetization Ms [emu/g]	Coercivity H_C [Oe]	Retentivity Mr [emu/g]	Anisotropic constant [K]
0	8.253	188.26	1.36	1585.41
0.2	15.087	120.99	0.14	1862.6
0.4	9.994	150.96	2.90	1539.48
0.6	8.781	102.22	2.85	915.91
0.8	6.725	61.328	1.73	420.84
1.0	0.110	16.226	0.341	1.821

Fig. 4. Hysteresis loops of $Cu_xCo_{1-x}Cr_{0.5}Fe_{1.5}O_4$.

In general, copper ferrites have partially inverse structure, in which 85 % of Cu^{+2} ions occupy octahedral sites, whereas other 15 % occupy the tetrahedral sites, whereas Fe^{3+} ions are equally distributed between these two sites [21] It means that Cu^{+2} ions have strong preference for octahedral sites. When Co ions are substituted by the Cu ions, cation distribution and the magnetic properties change subsequently. It can be observed that the saturation magnetization M_S has increased initially and then decreased. The initial increasing of the saturation magnetization M_S can be explained by Neel two-sublattice model [22]. In simple ferrites, the magnetic ordering is based on ferromagnetism model, in which the resultant magnetization is based on the difference between A-site and B-site magnetization. Furthermore, they are collinear and

antiparallel to each other. Hence, the interaction between A-site and B-site is the strongest and deeply predominates the A-A and B-B interactions. Thus, during the A-B interaction the magnetic spin in A-site aligns in one direction and in B-site in opposite direction. The Cu^{+2} ion with lesser magnetic moment sometimes occupy the A-site and force the Fe^{3+} ions to shift from B-site to A-site. As a result the net magnetization increases. The Neel two sub-lattice model is valid up to x = 0.2 and after that Yafet-Kittle model is appropriate.

According to this model the substitution of Cu^{+2} ions by Co^{2+} ions, which have preference to occupy the octahedral sites, results in reduction of exchange interaction between A and B sites or becomes comparable with B-B exchange interaction, which causes disturbances in the collinear structure of spin in B-sites of the system. So, this non collinear arrangement of the spin can cause a decrease in magnetization above x > 0.2. As the Cu^{+2} concentration increases, the magnetization of B site decreases. As a result, the dilution of spin on B-sites causes reduction of the net magnetization. On the other hand, this decreasing trend may be due to the lesser magnetic moment of a doped ion than that of the host ion. The magnetic moments of iron, copper and cobalt are 5 μ_B, 1 μ_B and 3 μ_B, respectively. As the Cu^{+2} ion has less magnetic moment as compared to Co^{2+} and Fe^{3+} ions, therefore, the saturation magnetization is observed to decrease with the substitution of Cu^{+2} ions. This behavior of saturation magnetization is also in accordance with crystallite size. Similarly, the value

Table 5. Observed and calculated magnetic moment/ formula unit and their respective model.

Sample (x)	M_{Cal} [μ_B/f·u]	M_{Obs} [μ_B/f·u]	Model fitted
0	3.2	5.73×10^{-2}	Neel model
0.2	3.6	10.5×10^{-2}	Neel model
0.4	2.9	6.97×10^{-2}	Yafet-Kittle model
0.6	2.8	6.13×10^{-2}	Yafet-Kittle model
0.8	2.6	4.73×10^{-2}	Yafet-Kittle model
1.0	1.6	7.77×10^{-5}	Yafet-Kittle model

Table 6. Bands gap and crystallite size for the samples of $Cu_xCo_{1-x}Cr_{0.5}Fe_{1.5}O_4$.

Sample x	Crystallite size D_p [nm]	Band gap energy E_g [eV]	Average grain size [nm]
0	12.62	1.91	730
0.2	47.11	1.92	600
0.4	59.72	1.94	380
0.6	47.11	1.93	300
0.8	48.71	1.94	280
1.0	10.50	2.12	200

of coercivity decreases with enhancement of Cu^{+2} content which can be explained on the basis of anisotropy and domain structure of the crystal [23]. Furthermore, in Wohlfarth theory the coercivity is linked with anisotropy constant by the following relation:

$$H_C = 0.98 \cdot K/M_S \quad (6)$$

where K is anisotropy constant and M_S is saturation magnetization [24]. It has been observed from Table 4 that anisotropy constant decreases from 1585.41 to 1.821 erg/Oe due to replacement of copper ions. As a result coercivity decreases and this decreasing behavior is attributed to weak spin - orbit coupling at B-site, which may be due to migration of Co^{2+} from octahedral site to tetrahedral site and hence, Fe^3 from tetrahedral site to octahedral site. The observed magnetic moment per formula unit in Bohr magneton has been calculated by using formula [24]:

$$M_{Obs} = (MW \cdot M_S)/5585 \quad (7)$$

where MW is the molecular weight of prepared samples and M_S is the saturation magnetization.

It is clear from Table 5 that the observed magnetic moment decreases with enhancement of copper concentration. The observed decrease in Bohr magneton is due to the decrease in A-B interaction.
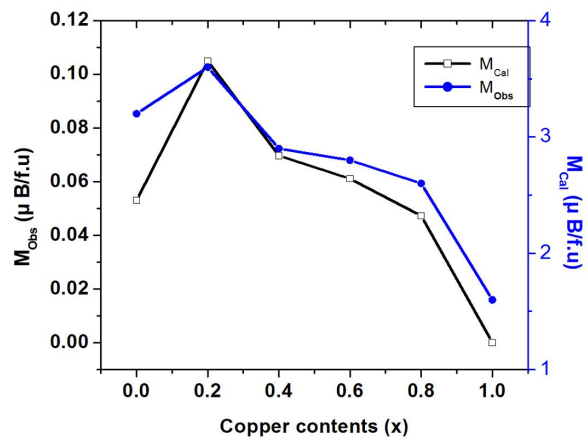

Fig. 5. Observed and calculated magnetic moment versus copper content x.

Similarly, the calculated value of magnetic moment per formula unit (M_{Cal}) is expressed as:
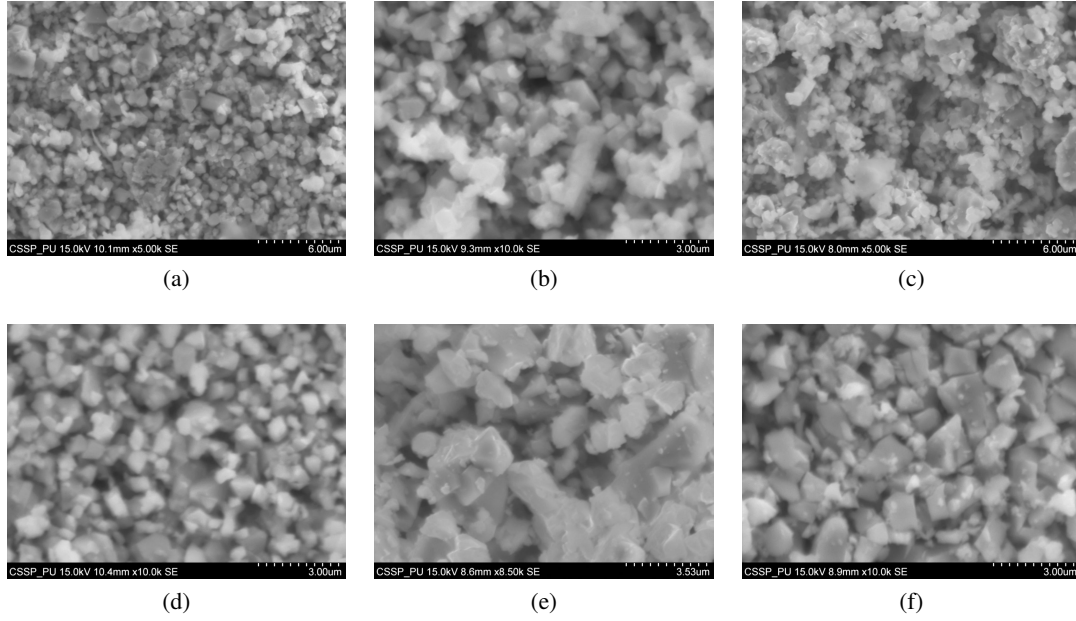
$$M_{Cal} = M_B(x) - M_A(x) \quad (8)$$

Fig. 6. SEM micrograph of $Cu_xCo_{1-x}Cr_{0.5}Fe_{1.5}O_4$: (a) at x = 0, (b) at x = 0.2, (c) at x = 0.4, (d) at x = 0.6, (e) at x = 0.8 and (f) at x = 1.
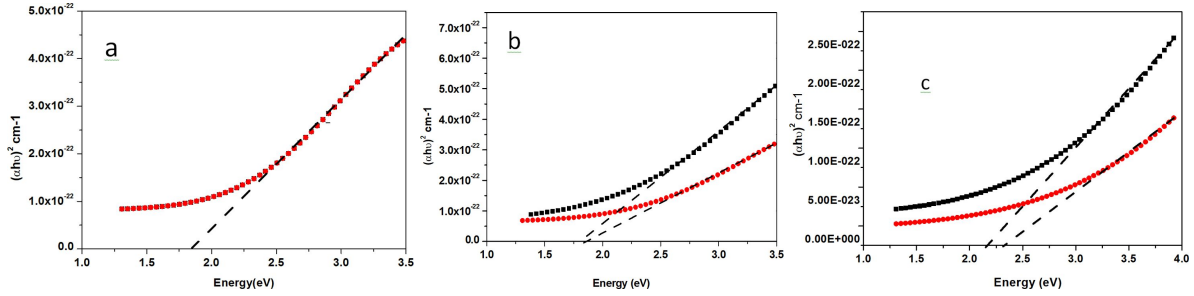

Fig. 7. Dependence of $(\alpha h\nu)^2$ versus phonon energy $h\nu$ for $Cu_xCo_{1-x}Cr_{0.5}Fe_{1.5}O_4$ with (a) x = 0, x = 0.2, (b) x = 0.4, x = 0.6, (c) x = 0.8, x = 1.

where M_A and M_B are the magnetic moments of A and B sublattice and their values have been calculated from cation distribution. For instance, at x = 0:

$$M_{Cal} = (Co_{0.7}Cr_{0.5}Fe_{0.8}) - (Co_{0.3}Fe_{0.7})M_{Cal}$$
$$= (0.7 \cdot 3 + 0.5 \cdot 3 + 0.8 \cdot 5) - (0.3 \cdot 3 + 0.7 \cdot 5)$$
$$= 3.2 \mu_B / f \cdot u$$

Similarly, the calculated value of magnetic moment per formula unit at x = 1.0 is:

$$M_{Cal} = (Cu_{0.7}Cr_{0.5}Fe_{0.8}) - (Cu_{0.1}Fe_{0.9})$$
$$= (0.7 \cdot 1 + 0.5 \cdot 3 + 0.8 \cdot 5) - (0.1 \cdot 1 + 0.9 \cdot 5)$$
$$= 1.6 \mu_B / f \cdot u$$

Both calculated and observed magnetic moments have decreasing trends and are shown in Fig. 5.

3.4. SEM analysis

Scanning electron microscopic technique has been used to study the microstructure and surface morphology of all ferrite samples as shown in Fig. 6.

It can be observed from the figures that the average grain size decreases with increasing copper concentration, which is due to the fact that the ionic radius of Cu^{+2} is smaller than that of Co^{+2}. Therefore, the decrease in grain size may be due to diffusion of copper during heat treatment.

From the observation of SEM, it is clear that ferrite samples are composed of a mixture of crystalline nanoparticles and grain agglomerates at high concentration of copper.

The average grain size calculated from SEM analysis has been tabulated in Table 6 and the similar result for the crystallite size has been obtained from XRD investigation.

3.5. UV-Vis analysis

The absorption spectra of the prepared samples have been recorded by UV-Vis spectrometer in the wavelength range of 200 nm to 800 nm. The optical absorption can be estimated on the basis of UV-Vis results from the relation between absorption coefficient, energy $h\nu$ and optical band gap:

$$\alpha h\nu = A(h\nu - E_g)^n \qquad (9)$$

where A is a constant which does not depend on $h\nu$, E_g is the band gap energy and n = 1 for direct band gap and n = 1/2 for indirect band gap material.

The band gap energy values have been calculated by plotting the graphs between $(\alpha h\nu)^2$ and E_g. The estimation of bad gap energy has been done by extrapolation of the linear part of the curve (Fig. 7). It has been observed from Fig. 7 that the value of E_g increases with the substitution of Cu^{2+} in the compound. Generally, an increase in band gap of Cu doped ferrite is due to a decrease in crystallite size which leads to Bras effective mass model [25, 26].

The band gap energy increases as the crystallite size decreases, which may be observed as the blue shift of absorption edge in absorption spectra. This causes the decrease in the number of overlapping energy levels. Thus, the increase of the gap between the valence and conduction bands results in an increase in the energy difference between these two bands.

It is revealed from Fig. 8 that the band gap energy increases with the decrease in crystallite size above the copper content above 0.6, and this behavior is also in good agreement with SEM results [18].
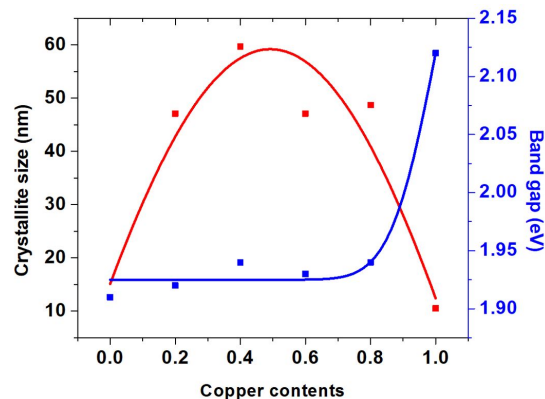

Fig. 8. Crystallite size and band gap energy versus copper content in $Cu_xCo_{1-x}Cr_{0.5}Fe_{1.5}O_4$.

4. Conclusions

The series of $Cu_xCo_{1-x}Cr_{0.5}Fe_{1.5}O_4$ ferrite samples with x = 0, 0.2, 0.4, 0.6, 0.8 and 1.0 have been successfully synthesized by standard double sintering ceramics technique. The X-ray diffraction patterns revealed the existence of a single phase cubic spinel structure in all ferrites sintered for 24 h at 1100 °C. XRD measurements depicted that the lattice parameter decreases with increasing the copper content in the ferrites due to the difference in ionic radii between Cu^{2+} and Co^{2+}. The X-ray density increases with increasing copper concentration. The cation distribution in the prepared ferrite is very complex. The IR spectral measurements indicated the presence of fundamental absorption bands υ_1 (662 to 657) and υ_2 (416 to 414) which have been formed in the range expected for a spinel type ferrite. Measurements of magnetic properties were done using VSM analysis which showed that the saturation magnetization and coercivity of the material decreased with increasing copper content. Therefore, the copper and cobalt mixed ferrites are useful for switching and memory devices.

References

[1] TARTAG P., MORALES M.D., SABIN V.V., *J. Appl. Phys.*, 36 (2003), 182.
[2] BADAR S.D., *J. Phys.*, 78 (2006), 1.
[3] ROSS C.A., *J. Mater. Res.*, 31 (2001), 203.
[4] WOOD R.W., MILES J., OLSON T., *IEEE T. Magn.*, 38 (2002), 1711.
[5] SWANT S.R., PATAIL R.N., *J. Appl. Phys.*, 20 (1982), 353.

[6] AHMAD I., ABBAS T., ISLAM M.U., MAQSOOD A., *J.Ceram. Int.*, 39 (2013), 6735.

[7] BRICEO S., CASTILLO H.D., SAGREDO V., BRAMER-ESCAMILLA W., SILVA P., *J. Surf. Sci.*, 263 (2012), 100.

[8] TAILHADES P., VILLETTE C., ROUSSET A., KULKARNI G., KANNAN K., RAO C., LENGLET M., *J. Solid State Chem.*, 141 (1998), 56.

[9] MATHEW T., SHIJU N., SREEKUMAR K., RAO B.S., GOPINATH C.S., *J.Catal.*, 210 (2002), 405.

[10] ABRAHAM T., *J. Ceram. Soc. Bull.*, 62 (1994), 73.

[11] CULLITY B.D., *Elements of X-ray Diffraction*, Addison Wesley, India, 1956.

[12] PECCHAL R.M., MADHURI W., RAMANANHAR R.N., SIVA KUMAR K.V., MURTHY V.R., RAMAKRISHNA R., *J. Sci. Eng.,* 30 (2010), 1094.

[13] GABAL M.A., AHMED M.A., *J Mater. Sci.*, 40 (2005), 388.

[14] SALAH L.M., MOUSTAFA A.M., AHMED FARAG I.S., *J. Ceram. Int.,* 38 (2012), 5605

[15] SHAIKH P.A., KAMBALE R.C., RAO A.V., KOLEKAR Y.D., *J. Alloy. Compd.*, 482 (2009), 276.

[16] BELAVI P.B., CHAVAN G.N., NAIK L.R., SOMASHEKAR R., KOTNALA R.K., *J. Mater Chem Phys.*, 132 (2012), 138.

[17] LADGAONKAR B.P., KOLEKAR C.B., VAINGANKAR A.S., *J. Mater. Sci.*, 25 (2002), 351.

[18] WALDRON R.D., *J. Phys. Rev.*, 99 (1955), 1727.

[19] PRADEEP A., PRIYADHARSINI P., CHANDRASEKARAN G., *J. Magn. Magn. Mater.*, 2774 (2008), 23.

[20] ZUO X., YANG A., VICTORIA C., HARRIS V.G., *J. Appl. Phys.*, 99 (2006), 909.

[21] NEEL L., *J. Phys.*, 3 (1948), 137.

[22] FARGH ALI AA., KHEDR MH, ABDEL KHALEK AA., *J. Mater. Process Technol.,* 81 (2007), 181.

[23] STONER E.C., WOHLFARTH E.P., PHILO S., *J. Trans. Magn.*, 27 (1991), 3475.

[24] LIN K.F., CHENG H.M., HSU H.C., LIN L., HSIEH W.F., *J. Chem. Phys. Lett.*, 409 (2005), 208.

[25] POLEZHAEVA O.S., YAROSHINSKAYA N.V., IVANOV V.K., *J. Inorg. Chem.,* 52 (2007), 1184.

[26] LIN H., HUANG C.P., LI W., NI C., SHAH S.I., TSENG Y.H., *J. Appl. Catal. B*, 68 (2006), 1.